Supplementary Figure Legends

Supplementary Figure 1. Transcriptomic analysis identifies four unique immune-related clusters A. Elbow plot showing optimal number of clusters in the data (k = 4). **B.** PCA plot showing distribution of DLBCLs from two independent data sources, indicating no batch effect (NCI – blue, UCMC – yellow). **C.** Bar plot quantifying distribution of cases from two independent data sources. **D-E.** Bar plots showing contribution of 19 immune-related and COO-related gene sets to PC1 **(D)** and PC2 **(E)**.

Supplementary Figure 2. Transcriptomic analysis identifies four unique immune-related clusters. A. PCA plot showing sample-wise GSVA enrichment scores for DLBCLs in an independent dataset (BCC). **B.** PCA biplot showing contribution of immune-related and COO-related gene sets to PC1 and PC2, respectively, for DLBCLs from the BCC dataset. **C**. PCA plot showing sample-wise GSVA enrichment scores for DLBCLs from all three datasets, colored by data source (NCI – blue, UCMC – yellow, BCC – red). **D.** Bar plot showing distribution of cases from NCI, UCMC, and BCC datasets within each GSVA-based immune cluster. **E**. PCA biplot showing contribution of immune-related and COO-related gene sets to PC1 and PC2 for DLBCLs in the combined NCI/UCMC/BCC dataset. **F**. PCA plot showing sample-wise GSVA enrichment scores for combined NCI/UCMC/BCC dataset.

Supplementary Figure 3. Validation of transcriptionally defined DLBCL-IQs. A. Heatmap showing estimated fraction of immune cell subtypes in each of the GSVA-based IQ as assessed by CIBERSORTx **B.** Violin plots showing absolute inferred proportions of $CD8^+$ T cells, conventional $CD4^+$ T cells, regulatory T cells (T_{regs}), and macrophages in each IQ as assessed by CIBERSORTx. **C.** Barplot of GSVA scores for immune-related gene sets for ABC hot compared to GCB hot (left) and ABC cold compared to GCB cold (right). **D.** Gene set enrichment analysis

(GSEA) plots for selected T cell exhaustion gene sets. Statistical analysis by Kruskal-Wallis test followed by a post-hoc Dunn's test with Benjamini-Hochberg (BH) adjusted p values. (NES – normalized enrichment score; ES – enrichment score).

Supplementary Figure 4. Prognostic significance of DLBCL-IQs. A-B. Progression free survival (PFS) **(A)** and overall survival (OS) **(B)** for DLBCLs assigned to the indicated IQs to R-CHOP chemoimmunotherapy. Log-rank test with Benjamini-Hochberg (BH)-adjusted p values.

Supplementary Figure 5. Concordance of DLBCL-IQs with other immune-related DLBCL subtypes. **A**. Alluvial plot demonstrating overlap between LME clusters and GSVA-defined DLBCL-IQs. **B.** Alluvial plot demonstrating overlap between LE clusters and GSVA-defined DLBCL-IQs. **C.** PCA plot (left) and bar plot (right) showing frequency of $DZsig^{+}$ DLBCLs in the NCI/BCC/UCMC cohort. (LME – Lymphoma microenvironment; GC – germinal center; ME – mesenchymal; IN – inflamed; DE – depleted; LE – Lymphoma ecotypes; DZsig - dark zone signature).

Supplementary Figure 6. Genomic features associated with DLBCL-IQs. A. Forest plot of genetic alterations recurrently associated with hot and cold DLBCL-IQs. Fisher's exact test with BH-adjusted p values displayed. (* adj. $p < 0.1$, ** adj. $p < 0.05$, *** adj. $p < 0.01$). **B.** Oncoprint (left) and bar plot (right) showing frequency of alterations in BCR-dependent NFκB pathway genes among the four DLBCL-IQs. **C.** Oncoprint (left) and bar plot (right) showing frequency of alterations in cell cycle genes genes among the four GSVA-defined immune-related clusters. Unadjusted p values displayed.

Supplementary Figure 7. MYC activity is associated with cold DLBCL immune environments. A. Bar plot showing frequency of MYC IHC^{+} DLBCLs in transcriptionally defined MYC-High, MYC-Int, MYC-Low groups. **B.** Box plot showing MYC score for DLBCLs in each GSVA-based immune related cluster. **C.** PCA plot (left) and bar plot (right) showing frequency of MYC-High DLBCLs in immune clusters. **D.** Heatmap showing absolute inferred proportions of immune cell subsets in MYC-High and MYC-Low DLBCLs from ABC and GCB clusters. **E-F.** Violin plots showing absolute inferred proportions of CD8^{+} **(E)** and CD4^{+} **(F)** T cells in MYC-High and MYC-Low DLBCLs in ABC and GCB clusters. **G.** Box plot showing CD8^{+}T cell : DLBCL ratio in MYC-High, MYC-Int, MYC-Low groups. **H.** Scatter plot showing correlation of MYCUp4 score and CD8^{+} T cell : DLBCL cell ratio. **I.** Box plot showing CD4+T cell : DLBCL ratio in MYC-High, MYC-Int, MYC-Low groups. **J.** Scatter plot showing correlation of MYC score and CD4^{+} T cell : DLBCL ratio. Fisher's exact test with BH-adjusted p values for comparison of categorical variables. Kruskal-Wallis test followed by post-hoc Dunn's test with adjusted p values for comparison of continuous variables.

Supplementary Figure 8. *SOCS1* mutations are enriched among GCB Hot DLBCLs and enhance B cell sensitivity to IFNγ signaling. A. Representative gating for splenocytes isolated from *Cd19*$^{Cre/+}$ or *Cd19*$^{Cre/+}$ *Socs1*$^{fl/fl}$ mice. **B.** Representative staining of H-2^{b}, I-A/I-E^{b}, and PD-L1 on CD19^{+} and CD3^{+} splenocytes from *Cd19*$^{Cre/+}$ or *Cd19*$^{Cre/+}$ *Socs1*$^{fl/fl}$ mice cultured with media or 100 ng/mL of IFNγ for 48 hours. **C.** Fold change in mean fluorescence intensity (MFI) of H-2^{b}, I-A/I-E^{b}, and PD-L1 on CD3^{+} splenocytes. Splenocytes from *Cd19*$^{Cre/+}$ (n = 6) or *Cd19*$^{Cre/+}$ *Socs1*$^{fl/fl}$ mice (n = 6) were cultured with media or the indicated concentrations of IFNγ for 48 hours and expression levels of H-2^{b}, I-A/I-E^{b}, and PD-L1 were measured. Mice were pooled from 3 independent biological replicates. Two-way ANOVA with Bonferroni correction, adj. p values displayed (* adj. $p < 0.05$, ** adj. $p < 0.01$, *** adj. $p < 0.001$, **** adj. $p < 0.0001$).

Supplementary Figure 9. DLBCL-IQs are associated with distinct survival outcomes to BsAb therapy but not CAR T cell treatment. **A.** PCA biplot showing the contribution of immune-related gene sets and COO-related gene sets to PC1 and PC2, respectively, for pre-treatment r/r DLBCL biopsies from patients treated with mosunetuzumab (N = 74). **B.** PFS for patients assigned to ABC Hot and ABC Cold DLBCL-IQs and treated with mosunetuzumab. Log-rank test with p value displayed. **C.** PCA biplot showing contribution of immune-related and COO-related gene sets to PC1 and PC2, respectively, for biopsies from patients treated with axi-cel in the Stanford cohort (N = 51).

Supplementary Figure 10. DLBCL-IQs are associated with distinct survival outcomes to BsAb therapy but not CAR T cell treatment. **A.** PCA biplot showing the contribution of immune-related gene sets and COO-related gene sets to PC1 and PC2, respectively, for pre-treatment r/r DLBCL biopsies from an independent cohort of patients treated with CD19 CAR T cell therapy (MSKCC, N = 69). **B.** PCA plot showing sample-wise GSVA enrichment scores for DLBCLs in the MSKCC cohort. **C.** PFS for patients assigned to "hot" or "cold" DLBCL immune clusters and treated with CD19 CAR T cell therapy (top) and forest plot showing hazard ratio of the association between PC1 score and PFS (bottom). Log-rank test with p value displayed. **D.** PFS for patients assigned to each DLBCL-IQ and treated with CD19 CAR T cell therapy in the MSKCC cohort. Log-rank test with p value displayed.

Supplementary Figure 1

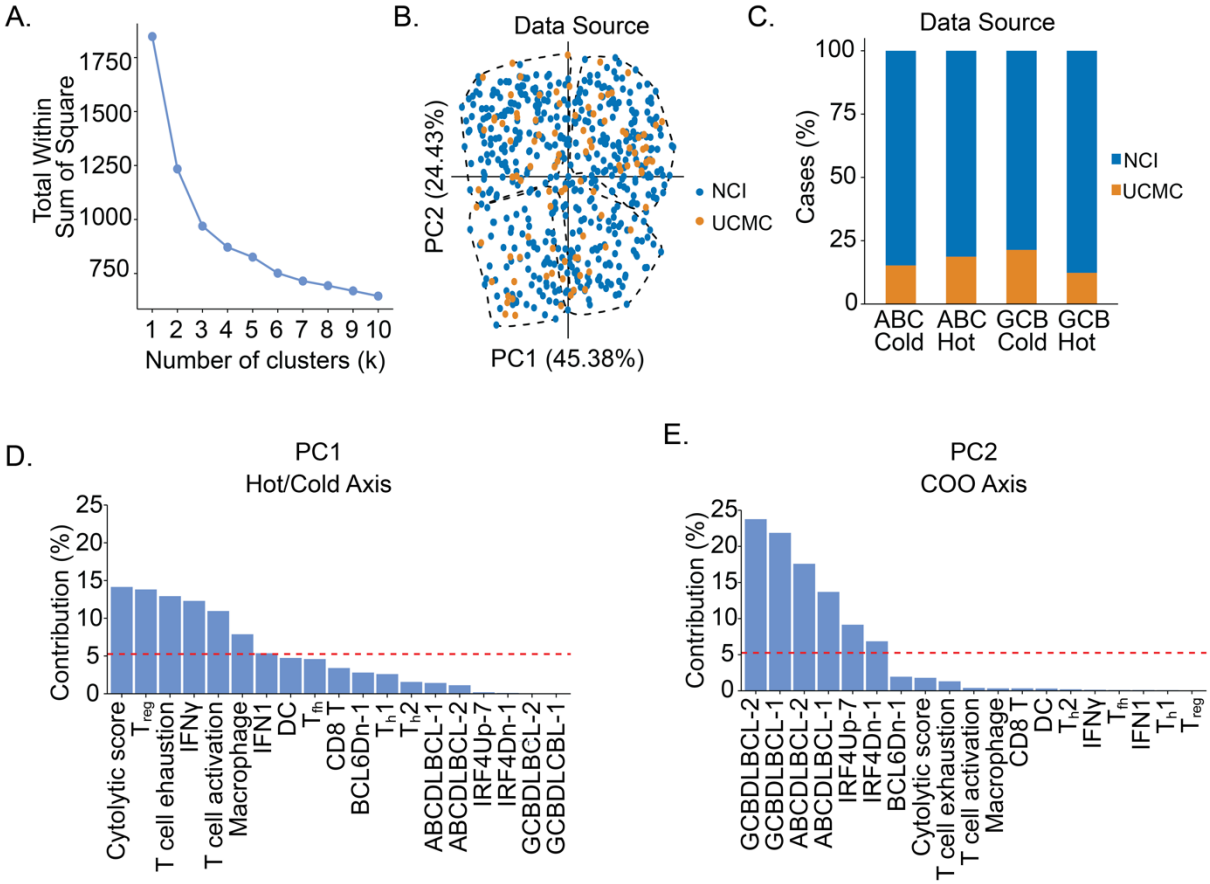

Supplementary Figure 2

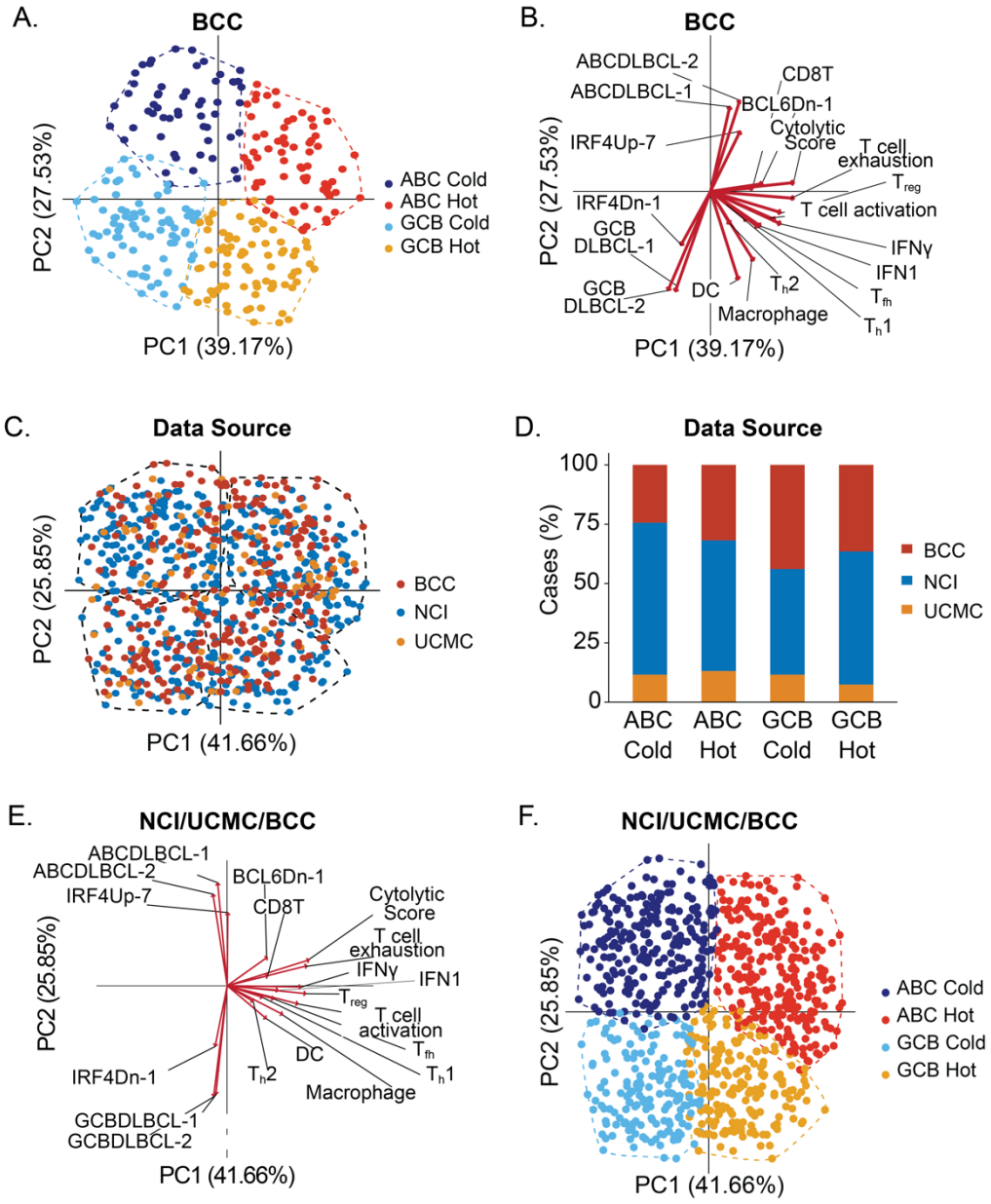

Supplmentary Figure 3

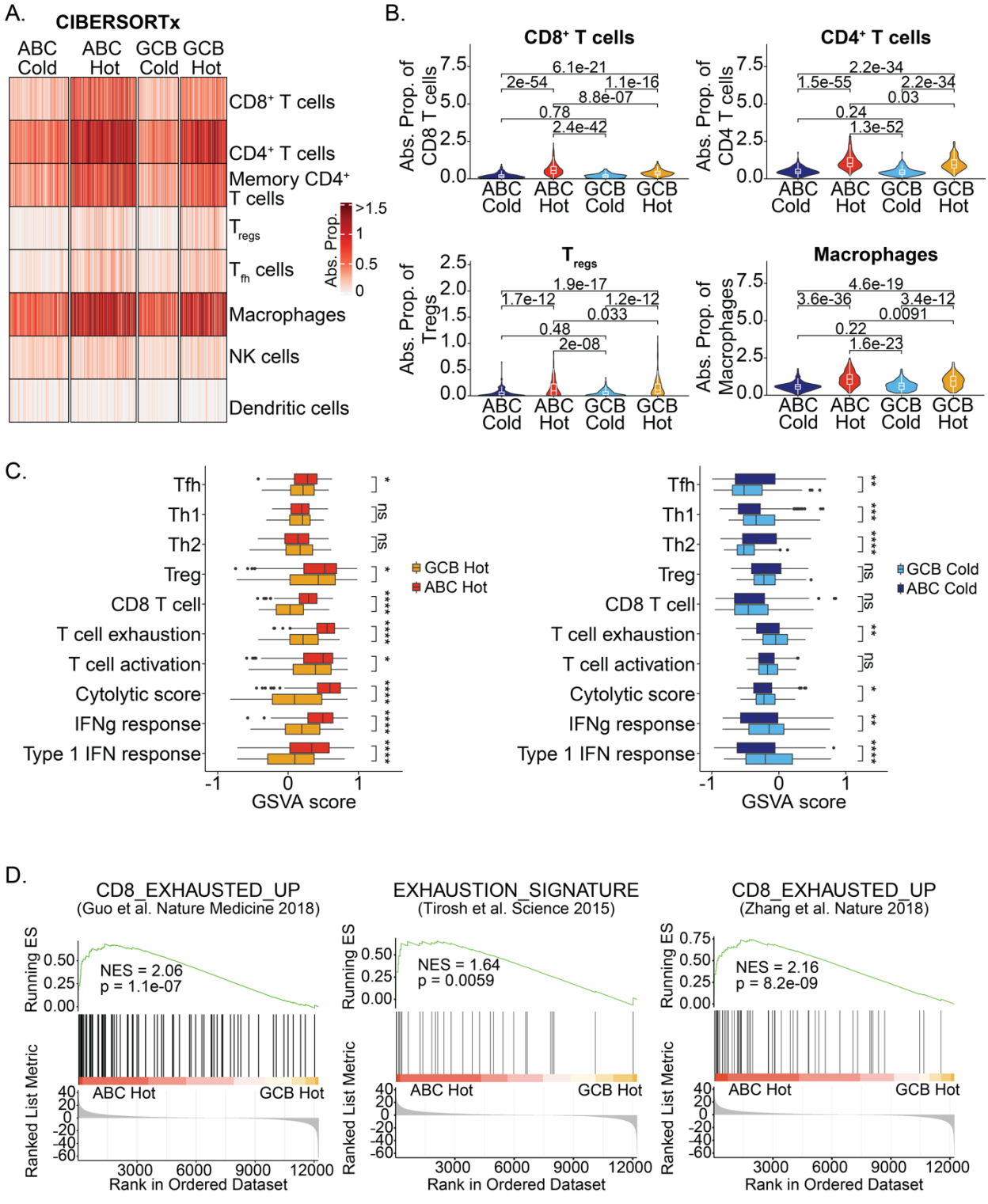

Supplementary Figure 4

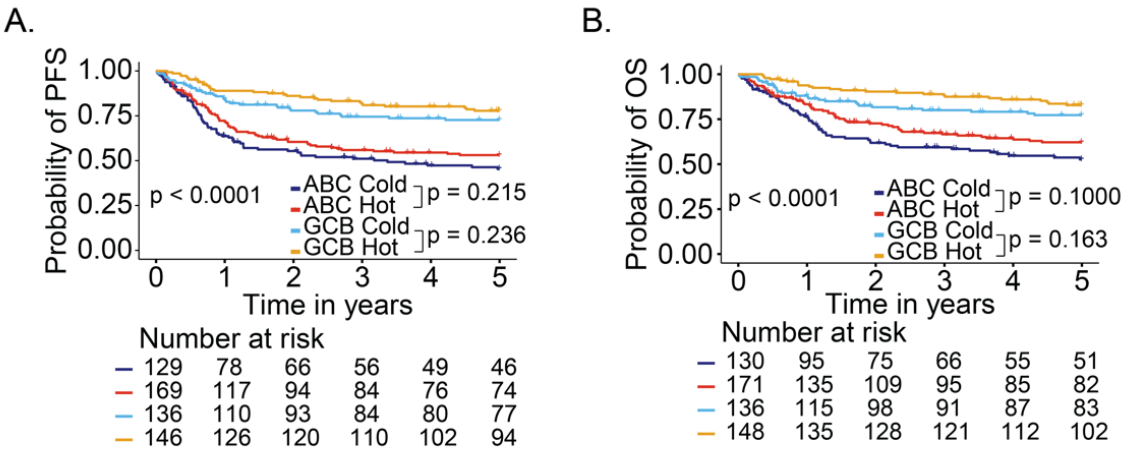

Supplementary Figure 5

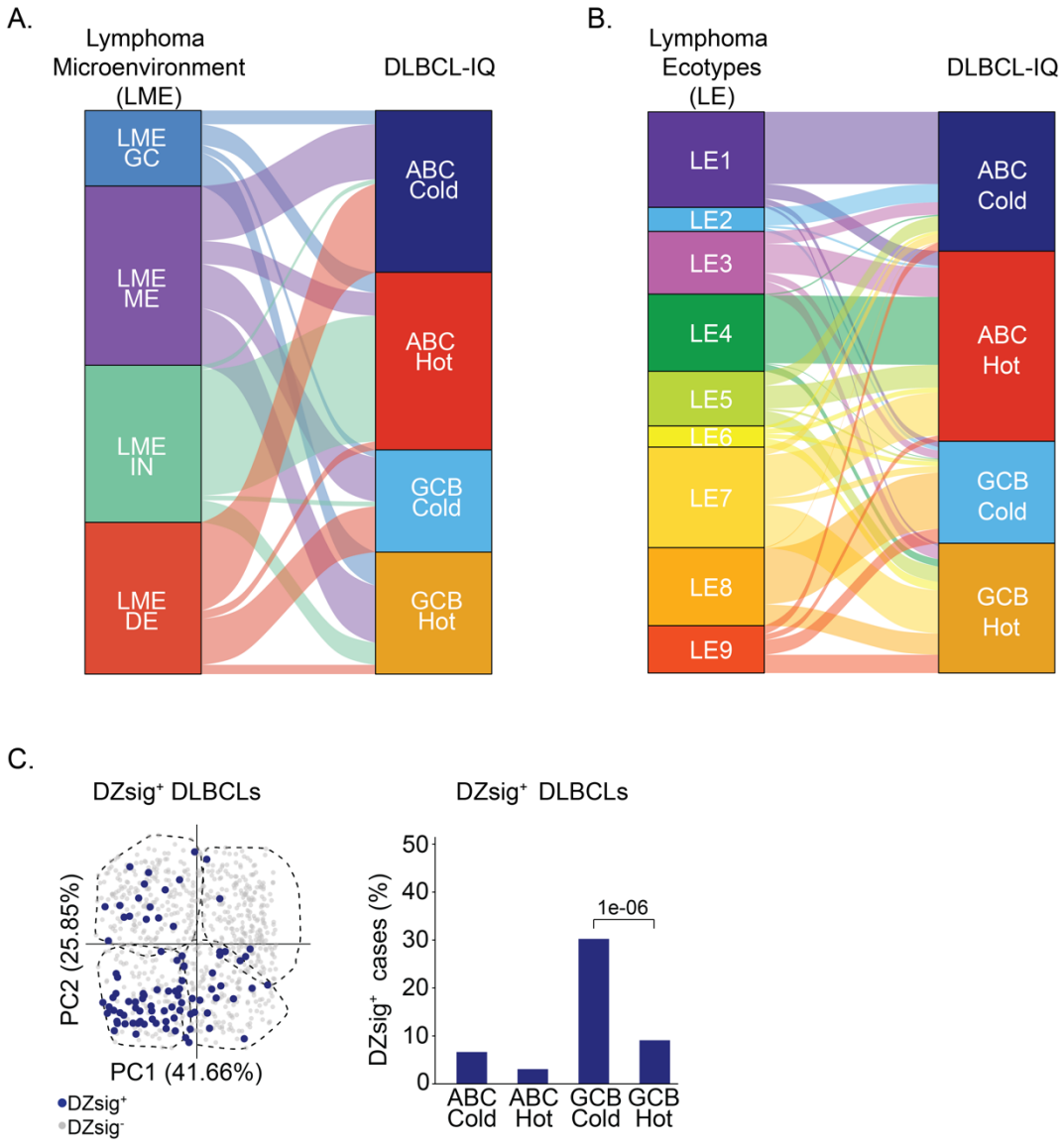

Supplementary Figure 6

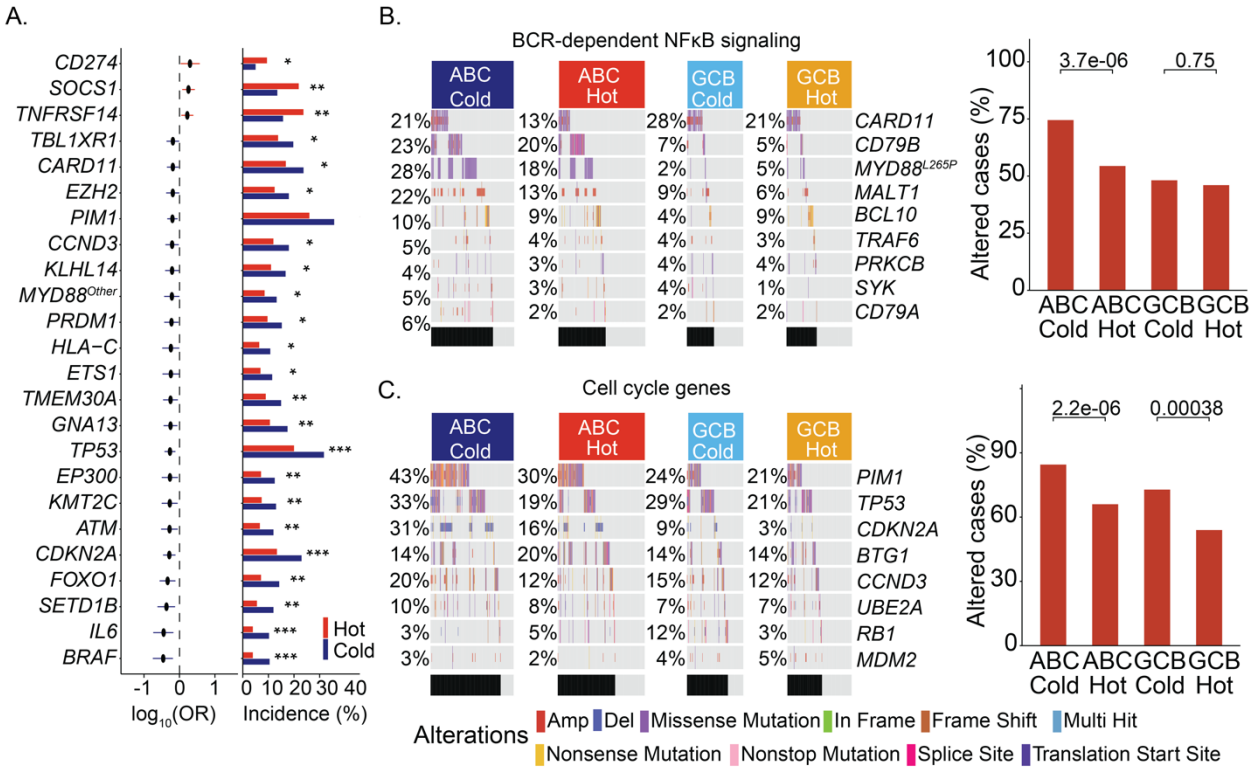

Supplementary Figure 7

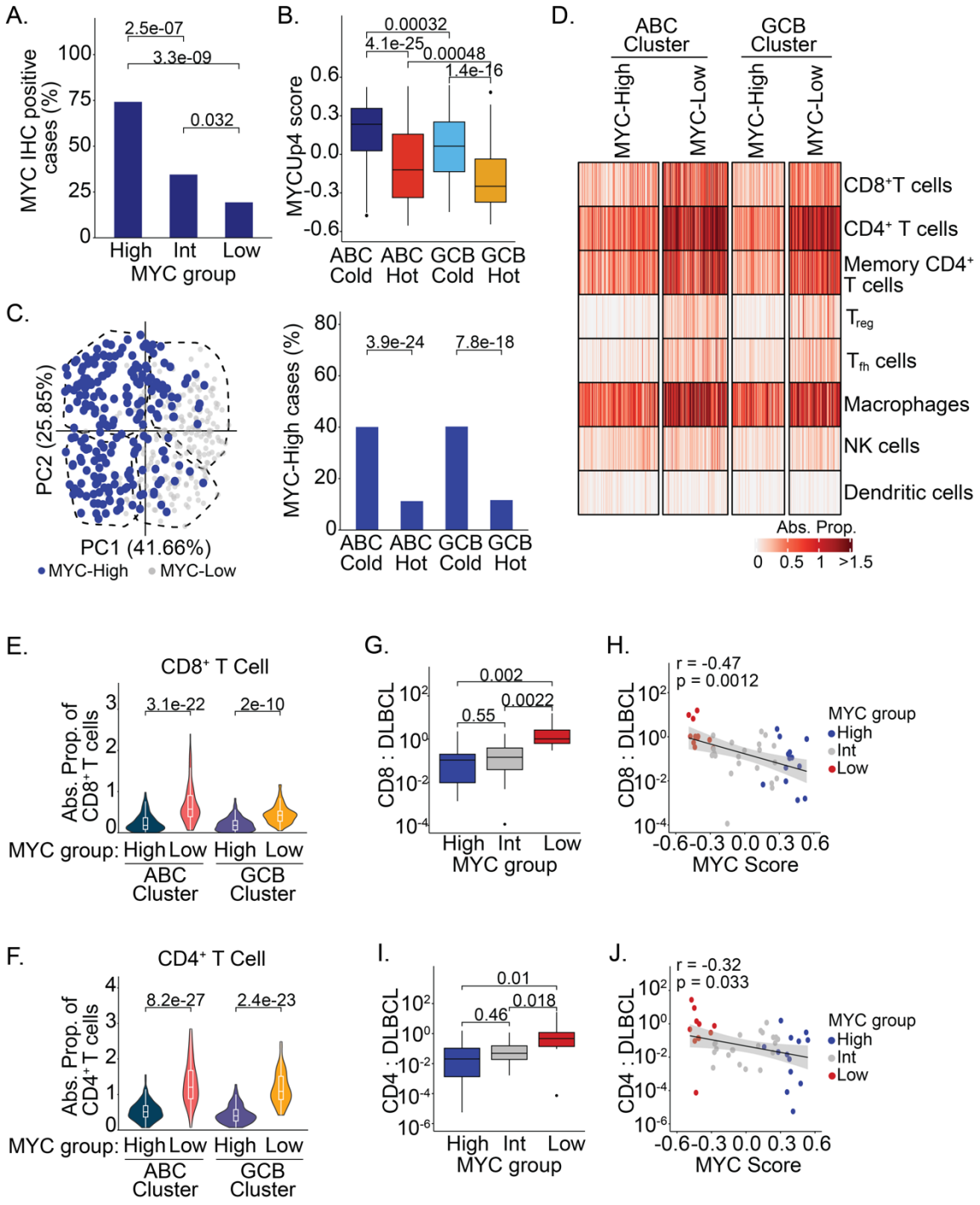

Supplementary Figure 8

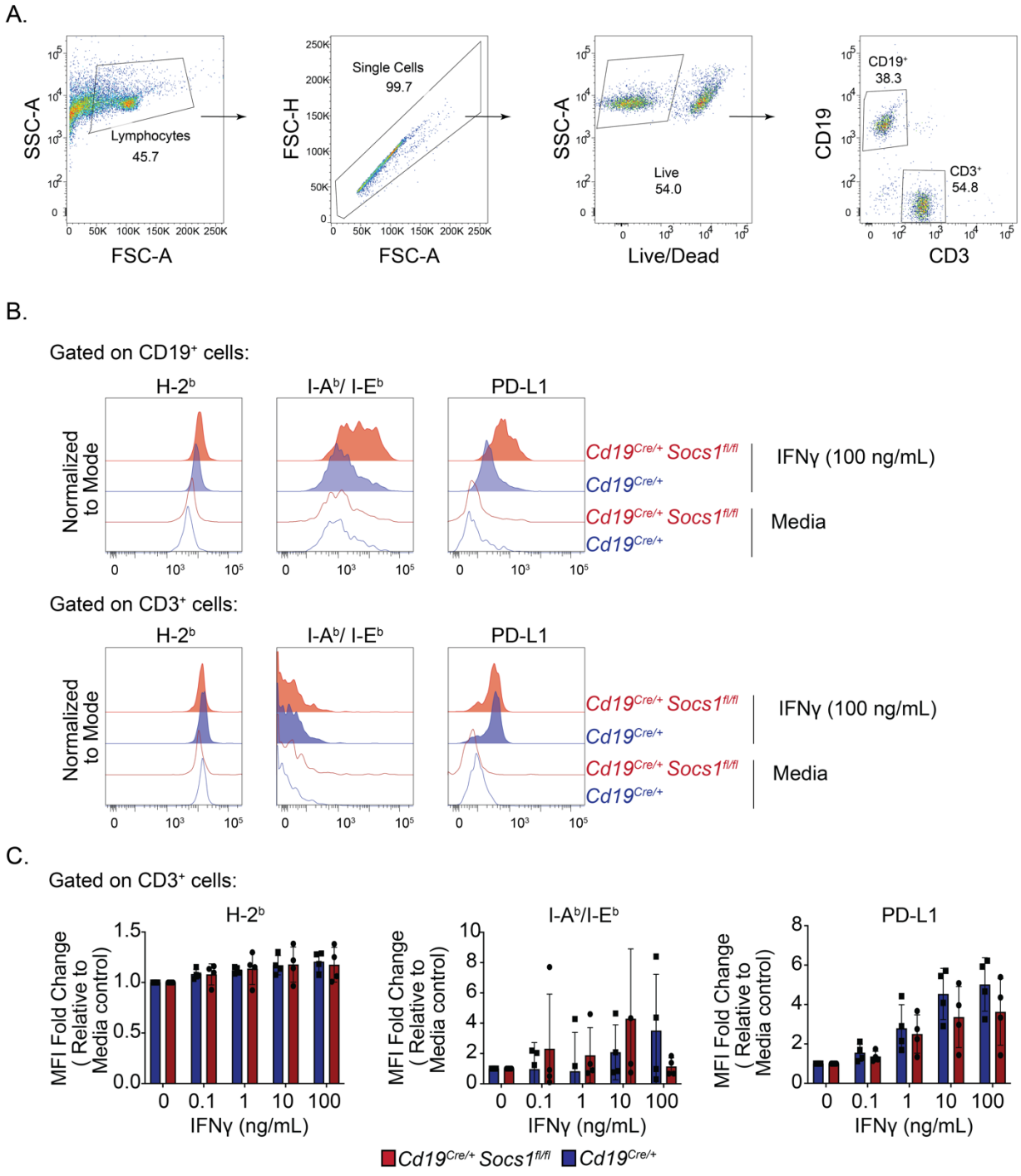

Supplementary Figure 9

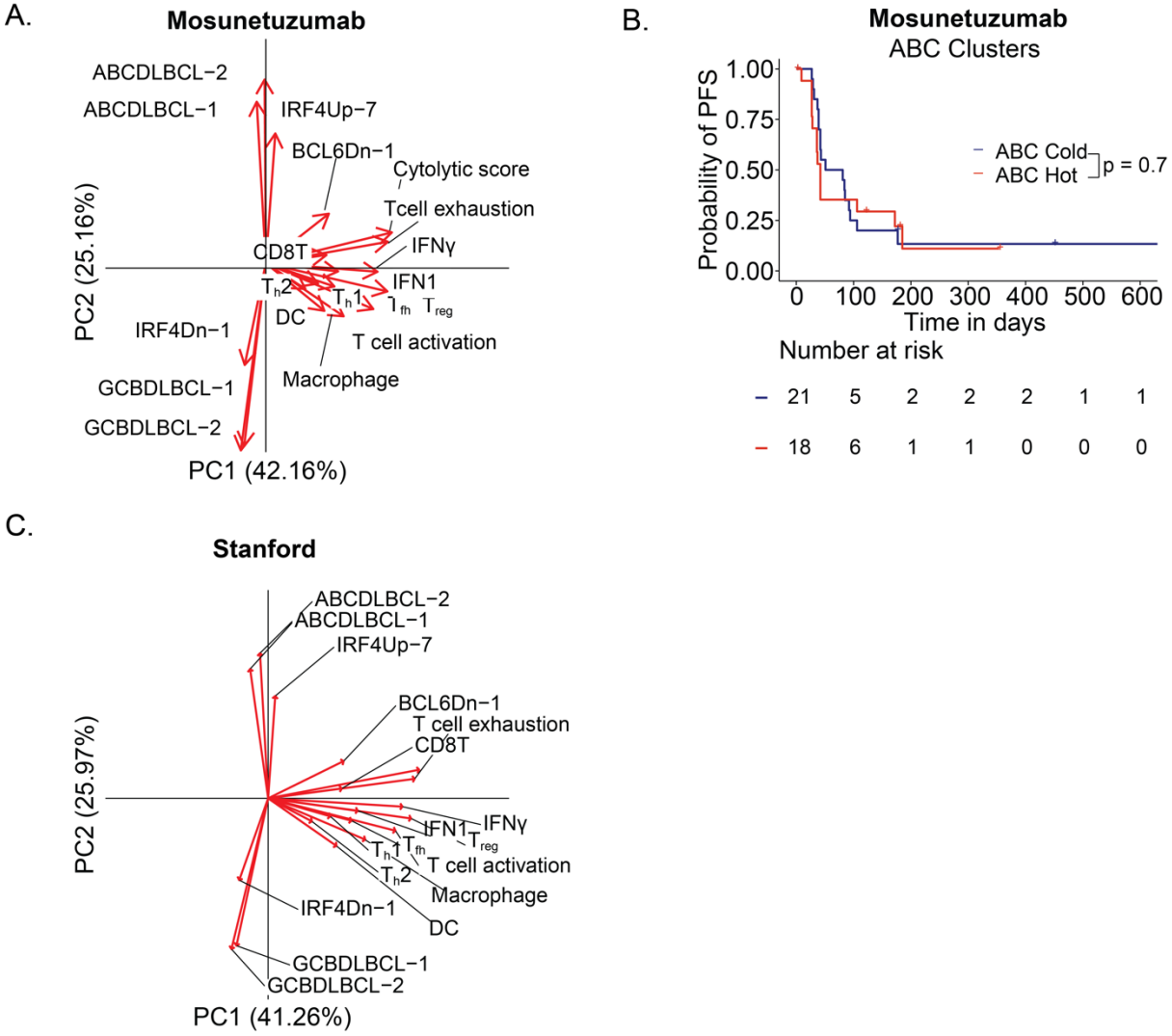

Supplementary Figure 10

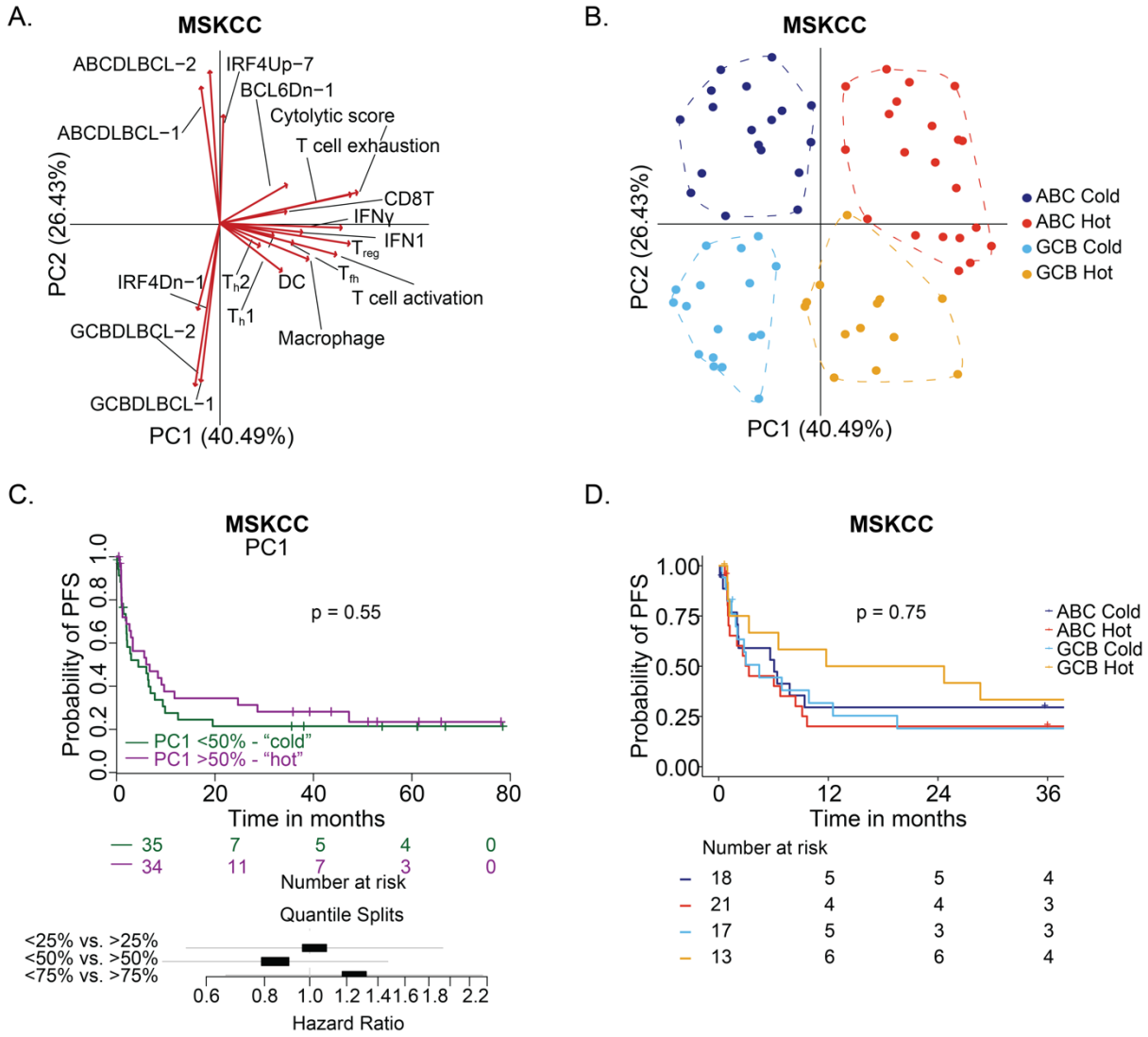

Supplementary Table 1. Description of DLBCL specimens and analyses performed

Datasets	RNA-Seq	WES/CNA	IHC/mIF
NCI	**481**	**481**	**N/A**
BCC	**285**	**283**	**~260 - IHC**
UCMC	**96**	**76**	**65 - mIF**
Mosunetuzumab	**74**	**N/A**	**N/A**
Stanford	**51**	**N/A**	**N/A**
MSKCC	**69**	**N/A**	**N/A**

WES- Whole exome sequencing; CNA – Copy number analysis; IHC – Immunohistochemistry; mIF – Multispectral immunofluorescence

Supplementary Table 2. List of genes included in GSVA analysis.

Gene Set	Genes
T cell exhaustion	*LAG3 CTLA4 CD274 CD160 BTLA VSIR LAIR1 HAVCR2 CD244 TIGIT*
T cell activation	*ICOS CD28 CD27 TNFSF14 CD40LG TNFRSF9 TNFRSF4 TNFRSF25 TNFRSF18 TNFRSF8 SLAMF1 CD2 CD226*
Cytolytic score	*GZMA GZMH GZMM PRF1 GNLY*
Interferon gamma	*TIGIT CXCR6 CXCL9 CD27 CMKLR1 HLA-DQA1 CD8A NKG7 CD276 PDCD1LG2 CCL5 STAT1 LAG3 PSMB10 HLA-DRB1 CD274 IDO1 HLA-E*
IFN-1	*MX1 TNFSF10 RSAD2 IFIT1 IFIT3 IFIT2 IRF7 DDX4 MX2 ISG20*
CD8T	*ADRM1 AHSA1 C1GALT1C1 CCT6B CD37 CD3D CD3E CD3G CD69 CD8A CETN3 CSE1L GEMIN6 GNLY GPT2 GZMA GZMH GZMK IL2RB LCK MPZL1 NKG7 PIK3IP1 PTRH2 TIMM13 ZAP70*
Regulatory T cell	*FOXP3 LINC02694 IL5 CTLA4 IL32 GPR15 IL4*
T_h2	*ASB2 CSRP2 DAPK1 DLC1 DNAJC12 DUSP6 GNAI1 LAMP3 NRP2 OSBPL1A PDE4B PHLDA1 PLA2G4A RAB27B RBMS3 RNF125 TMPRSS3 GATA3 BIRC5 CDC25C CDC7 CENPF CXCR6 DHFR EVI5 GSTA4 HELLS IL26 LAIR2*
Th1	*CD70 TBX21 ADAM8 AHCYL2 ALCAM B3GALNT1 BBS12 BST1 CD151 CD47 CD48 CD52 CD53 CD59 CD6 CD68 CD7 CD96 CFHR3 CHRM3 CLEC7A COL23A1 COL4A4 COL5A3 DAB1 DLEU7 DOC2B EMP1 F12 FURIN GAB3 GATM GFPT2 GPR25 GREM2 HAVCR1 HSD11B1 HUNK IGF2 RCSD1 RYR1 SAV1 SELE SELP SH3KBP1 SIT1 SLC35B3 SIGLEC10 SKAP1 THUMPD2 TIGIT ZEB2 ENC1 RETREG1 FBXO30 FCGR2C STAC LTC4S MAN1B1 MDH1 MMD RGS16 IL12A P2RX5 ADGRE5 ITGB4 ICAM3 METRNL TNFRSF1A IRF1 HTR2B CALD1 MOCOS TRAF3IP2 TLR8 TRAF1 DUSP14*
T follicular helper	*B3GAT1 CDK5R1 PDCD1 BCL6 CD200 CD83 CD84 FGF2 GPR18 CEBPA ADA2 CLEC10A CLEC4A CSF1R CTSS SYNM DPP4 LRRC32 MC5R MICA NCAM1 NCR2 NRP1 PDCD1LG2 PDCD6 PRDX1 RAE1 RAET1E SIGLEC7 SIGLEC9 TYRO3 CHST12 CLIC3 IVNS1ABP KIR2DL2 LGMN*
Macrophage	*FUCA1 MMP9 LGMN HS3ST2 TM4SF19 CLEC5A GPNMB KCNJ5-AS1 CD68 CYBB*
Dendritic cell	*CD1A CD1B CD1E CCL13 CCL17 ALDH1A2 CD209 ALOX15 HLA-DQA1 FPR3*
ABCDLBCL-1	*ACP1 BATF BCL2 CCND2 CSNK1E ENTPD1 FUT8 GOT2 IGHG1 IL16 IRF4 MARCKS PIM1 PIM2 PRKCB PTPN1 SLA SP140 SPIB TCF4*

ABCDLBCL-2	*BLNK BMF CCDC50 CCND2 ENTPD1 ETV6 FOXP1 FUT8 IGHM IL16 IRF4 PIM1 PTPN1 SH3BP5 TBC1D27P*
GCBDLBCL-1	*BCL6 CSTB FAM3C ITPKB LMO2 IRAG2 MME MYBL1 SPINK2 VCL*
GCBDLBCL-2	*BCL6 DENND3 ITPKB LMO2 IRAG2 MME MYBL1 NEK6 SAMD12 SERPINA9*
IRF4Up7	*ALAD ANKRD33B ARHGAP17 ARHGAP24 ARHGAP25 ARHGAP31 ARHGEF3 ARID3A ASPHD2 ATP1B1 AURKA BATF BCL2 BCL3 BLNK BMF BSPRY RHEX CABLES1 CARD11 CCDC113 CCDC88C CCL22 CCND2 CD47 CDKL1 CFLAR CLINT1 COL9A2 CORO1C CSNK1E CXXC5 CYB5R2 DCTD DGKG DHRS9 DNAJC25-GNG10 DOCK10 DUSP15 DUSP5 EHD1 EHD3 EIF2S2 ELL2 ELOVL7 ENTPD1 ERP29 ETV6 FA2H FCMR FCRL5 FKBP11 FOXP1 GAB2 GID4 GYG1 HCK HIVEP2 HSP90B1 IDH1 IL10 IL16 IQGAP2 IRF2 IRF2BP2 IVNS1ABP KLHDC9 KRAS LBH LDLR LYN MAP3K5 MAPKAPK2 MARS1 MLKL MOCOS MPEG1 MSRB1 MYOCD NCF2 NDRG1 NFKBIZ NRROS OAS1 PAK2 PARVB PDCD4 PDE4B PDLIM1 PHACTR2 PIAS2 PIGR PIM1 PNP POU2F2 PPFIBP2 PRDM2 PRPF40A PTPN1 RAC2 RAPGEF1 RARA RASGRP4 RHOQ RILPL2 RUBCNL S1PR1 SACS SCD SEC11C SERPINB8 SFTPB SH2D3C SH3BP1 SH3BP5 SIDT1 SKIL SLA SLC25A30 SLC33A1 SLC39A10 SLC4A5 SMARCA2 SNX9 SP140 SPIB SPTBN1 SSR3 ST3GAL1 ST6GALNAC4 STAMBPL1 STAT3 TCF4 TCTN3 TET2 TLE1 TMEM154 TNFAIP8 TOX2 TPM4 TRAM2 TREX1 UBALD2 UCK2 UNC93B1 VASH2 VAV2 VEGFA VOPP1 WNT10A WNT9A YARS1 ZBTB32 ZFAT ZNF432*
IRF4Dn1	*ADGRG5 AIM2 ALOX5AP ANK1 ANK3 ARHGAP44 ARL5B ATL2 BCAS4 BFSP2 BICD1 BORCS8-MEF2B BPTF SHLD1 CCDC126 CCDC69 CCND3 CD1A CD27 CD38 CD83 CD86 CDK14 CEP126 CFAP58 CLIC5 COA1 COTL1 CUX1 CYP39A1 DAAM1 DEF8 DHRS9 DIP2C DOK3 EBF1 EHD3 ELF1 EML6 ENPP3 EPSTI1 ERP44 FAM53B FANCA FCRL1 FCRLB GATAD2B GCNT1 GCSAM GPR160 HECW2 HGSNAT HSD17B12 HTR3A IGSF22 ILDR1 IQCD ITPKB IZUMO4 KCNN3 GARRE1 KIAA1549L KLF12 KLHL6 KRT13 LACC1 LCK LHPP LNPEP LPP IRAG2 LY9 LYL1 MAP3K7CL MAP4K4 MAST3 MBD4 MCTP2 MED12L MEF2C MET MILR1 MOB1A MOB3A MPZL3 MTF2 MYO1E NCALD NCOA7 NLRP2 NR3C1 OTULIN PACSIN1 PAG1 PALD1 PHLPP1 PIK3CG PIP4K2A PITPNC1 PLAG1 PLXNB2 POLD4 POLH PPIL2 PRAG1 PRKCD PRKRIP1 PTAFR PTK2B PTPN18 PTPRS PUDP PXK RCBTB2 RECQL5 REL RFTN1 RRM2B S1PR2 SEC14L1 SEMA4A SGPP1*

	SH2B2 SH3KBP1 SLC15A4 SLC25A27 SLC2A5 SLC6A16 SMARCA4 SMIM14 SOBP SOX5 SPRED2 STAG3 STX7 SWAP70 SYK SYNE2 SYT11 TBC1D4 TMEM123 TMEM131L TMEM229B TNFSF10 TOB2 TPCN1 TPCN2 UBE2J1 USP12 VGLL4 WIPI2 XKR6 XYLT1 ZFHX3 ZNF318 ZNF581 ZNF608
BCL6Dn-1	*ATR CCL3 CCND2 CD44 CD69 CD80 CDKN1A CDKN1B CXCL10 CXCR4 GPR183 ID2 IFITM1 IFITM3 IRF9 NFKB1 PRDM1 STAT1 TP53*

Supplementary Table 3. Frequency and number of DLBCL driver genes in NCI, UCMC, and BCC datasets.

HUGO Symbol	NCI-UCMC-BCC (%)	NCI-UCMC-BCC (n)	NCI (%)	NCI (n)	UCMC (%)	UCMC (n)	BCC (%)	BCC (n)
KMT2D	37.26	313	34.51	166	21.05	16	46.28	131
PIM1	30.47	256	30.76	148	17.1	13	33.56	95
BCL2	27.73	233	26.19	126	13.15	10	34.27	97
TP53	25.47	214	27.23	131	19.73	15	24.02	68
MYD88	24.04	202	27.65	133	21.05	16	18.72	53
CREBBP	22.26	187	20.79	100	22.36	17	24.73	70
BTG2	21.66	182	23.07	111	9.21	7	22.61	64
CARD11	20	168	18.5	89	15.78	12	23.67	67
H1-4	20	168	19.54	94	17.1	13	21.55	61
TNFRSF14	19.76	166	18.5	89	18.42	14	22.26	63
TNFAIP3	18.8	158	25.36	122	10.52	8	9.89	28
B2M	17.97	151	17.46	84	13.15	10	20.14	57
BCL6	17.97	151	20.99	101	3.94	3	16.6	47
CDKN2A	17.85	150	27.02	130	25	19	0.35	1
SOCS1	17.73	149	15.17	73	18.42	14	21.9	62
TMSB4X	17.26	145	19.33	93	5.26	4	16.96	48
IRF4	17.02	143	15.38	74	18.42	14	19.43	55
KLHL6	17.02	143	17.46	84	6.57	5	19.08	54
HLA-B	16.9	142	24.32	117	23.68	18	2.47	7
TBL1XR1	16.54	139	20.16	97	5.26	4	13.42	38
BTG1	15.83	133	15.38	74	9.21	7	18.37	52
SGK1	15.71	132	16	77	5.26	4	18.02	51
CD79B	15.11	127	15.17	73	19.73	15	13.78	39
EZH2	15	126	13.3	64	7.89	6	19.78	56
CCND3	14.76	124	16.63	80	14.47	11	11.66	33
ACTB	14.28	120	11.64	56	13.15	10	19.08	54
H1-2	14.28	120	12.26	59	15.78	12	17.31	49
GNA13	13.8	116	9.97	48	10.52	8	21.2	60
KLHL14	13.69	115	18.5	89	9.21	7	6.71	19
HLA-A	13.21	111	17.87	86	23.68	18	2.47	7
ZFP36L1	13.09	110	11.01	53	9.21	7	17.66	50
CD58	12.85	108	15.17	73	5.26	4	10.95	31
MEF2B	12.61	106	10.18	49	7.89	6	18.02	51
BCL11A	12.26	103	12.88	62	9.21	7	12.01	34
PRDM1	12.26	103	16.21	78	13.15	10	5.3	15

CD70	11.9	100	16	77	6.57	5	6.36	18
IRF8	11.78	99	12.26	59	6.57	5	12.36	35
TMEM30A	11.78	99	13.09	63	1.31	1	12.36	35
DTX1	11.3	95	17.25	83	9.21	7	1.76	5
MYC	11.07	93	9.77	47	13.15	10	12.72	36
ARID1A	10.83	91	11.43	55	3.94	3	11.66	33
EBF1	10.83	91	10.81	52	NA	NA	13.78	39
FOXO1	10.47	88	9.35	45	2.63	2	14.48	41
XPO1	10.47	88	10.6	51	17.1	13	8.48	24
FAS	10.23	86	11.43	55	5.26	4	9.54	27
NFKBIE	10.23	86	11.01	53	5.26	4	10.24	29
KMT2C	10	84	7.48	36	3.94	3	15.9	45
SPEN	10	84	12.05	58	3.94	3	8.12	23
EP300	9.64	81	9.97	48	5.26	4	10.24	29
PDE4DIP	9.52	80	12.47	60	3.94	3	6	17
CIITA	9.4	79	8.1	39	14.47	11	10.24	29
MCL1	9.28	78	9.14	44	19.73	15	6.71	19
STAT3	9.28	78	10.39	50	3.94	3	8.83	25
ATM	9.16	77	8.73	42	3.94	3	11.3	32
ETS1	9.04	76	11.85	57	3.94	3	5.65	16
CD83	8.8	74	6.65	32	10.52	8	12.01	34
BCL10	8.57	72	11.85	57	1.31	1	4.94	14
H1-5	8.57	72	11.64	56	13.15	10	2.12	6
SETD1B	8.57	72	11.85	57	11.84	9	2.12	6
HLA-C	8.45	71	10.81	52	18.42	14	1.76	5
ETV6	8.33	70	12.26	59	9.21	7	1.41	4
POU2F2	8.21	69	9.77	47	7.89	6	5.65	16
UBE2A	8.09	68	13.72	66	2.63	2	NA	NA
DUSP2	7.85	66	12.26	59	7.89	6	0.35	1
H2BC5	7.85	66	11.01	53	9.21	7	2.12	6
LTB	7.85	66	10.18	49	13.15	10	2.47	7
ATR	7.73	65	9.97	48	2.63	2	5.3	15
BIRC6	7.73	65	6.44	31	6.57	5	10.24	29
DDX3X	7.73	65	9.35	45	1.31	1	6.71	19
GNAI2	7.5	63	10.81	52	3.94	3	2.82	8
ZC3H12A	7.5	63	7.27	35	15.78	12	5.65	16
CD274	7.26	61	8.73	42	10.52	8	3.88	11
H2AC17	7.14	60	9.56	46	10.52	8	2.12	6
ARID1B	7.02	59	11.22	54	3.94	3	0.7	2
BRAF	7.02	59	7.48	36	NA	NA	8.12	23
CHST2	7.02	59	8.31	40	3.94	3	5.65	16
PAX5	7.02	59	10.81	52	6.57	5	0.7	2

IL6	6.9	58	6.02	29	5.26	4	8.83	25
POU2AF1	6.9	58	7.48	36	9.21	7	5.3	15
RHOA	6.9	58	7.9	38	2.63	2	6.36	18
TOX	6.9	58	11.01	53	2.63	2	1.06	3
H1-3	6.78	57	9.14	44	10.52	8	1.76	5
H2AC6	6.78	57	9.14	44	9.21	7	2.12	6
NAV1	6.78	57	6.44	31	3.94	3	8.12	23
NOTCH2	6.66	56	9.97	48	9.21	7	0.35	1
CBLB	6.42	54	7.9	38	2.63	2	4.94	14
FOXP1	6.42	54	7.48	36	7.89	6	4.24	12
MECOM	6.42	54	7.48	36	3.94	3	5.3	15
PIM2	6.42	54	10.81	52	2.63	2	NA	NA
RB1	6.42	54	5.61	27	NA	NA	9.54	27
SETD2	6.42	54	7.48	36	1.31	1	6	17
H2BC21	6.3	53	6.23	30	9.21	7	5.65	16
STAT6	6.19	52	5.82	28	7.89	6	6.36	18
CDC73	6.07	51	6.02	29	6.57	5	6	17
NFKBIA	6.07	51	5.19	25	6.57	5	7.42	21
BCL7A	5.83	49	6.86	33	9.21	7	3.18	9
DCAF6	5.83	49	5.19	25	9.21	7	6	17
H2BC12	5.83	49	7.27	35	10.52	8	2.12	6
TIPARP	5.83	49	7.27	35	2.63	2	4.24	12
HLA-DMA	5.71	48	5.82	28	17.1	13	2.47	7
MGA	5.71	48	9.77	47	1.31	1	NA	NA
NCOR1	5.71	48	8.31	40	6.57	5	1.06	3
BRINP3	5.59	47	5.19	25	6.57	5	6	17
MET	5.59	47	6.02	29	1.31	1	6	17
TET2	5.47	46	8.31	40	5.26	4	0.7	2
KRAS	5.35	45	5.61	27	2.63	2	5.65	16
SETD5	5.23	44	7.06	34	2.63	2	2.82	8
ZNF292	5.23	44	8.52	41	2.63	2	0.35	1
BTK	5.11	43	8.31	40	3.94	3	NA	NA
H3C2	5.11	43	3.95	19	10.52	8	5.65	16
HNRNPU	5.11	43	6.65	32	2.63	2	3.18	9
NLRP8	5	42	5.19	25	9.21	7	3.53	10
SIN3A	5	42	5.82	28	1.31	1	4.59	13
PTPN6	4.88	41	6.23	30	7.89	6	1.76	5
S1PR2	4.88	41	4.15	20	7.89	6	5.3	15
DDX10	4.76	40	6.02	29	1.31	1	3.53	10
EEF1A1	4.76	40	7.48	36	1.31	1	1.06	3
INO80	4.76	40	7.48	36	5.26	4	NA	NA
MARK1	4.64	39	5.19	25	3.94	3	3.88	11

TAF1	4.64	39	7.69	37	2.63	2	NA	NA
ZEB2	4.64	39	7.06	34	3.94	3	0.7	2
ZFAT	4.64	39	4.78	23	6.57	5	3.88	11
CRIP1	4.52	38	3.11	15	9.21	7	5.65	16
ZNF608	4.52	38	6.65	32	2.63	2	1.41	4
IKZF3	4.28	36	5.61	27	2.63	2	2.47	7
MAGT1	4.28	36	7.06	34	2.63	2	NA	NA
MYB	4.28	36	7.06	34	2.63	2	NA	NA
PHF6	4.28	36	6.23	30	1.31	1	1.76	5
PRKCB	4.16	35	6.02	29	2.63	2	1.41	4
PTPRK	4.16	35	7.06	34	1.31	1	NA	NA
TGFBR2	4.16	35	4.57	22	1.31	1	4.24	12
WAC	4.16	35	5.61	27	5.26	4	1.41	4
ZFX	4.16	35	7.06	34	1.31	1	NA	NA
IL16	4.04	34	6.23	30	3.94	3	0.35	1
MSH6	4.04	34	4.57	22	2.63	2	3.53	10
PIK3CD	4.04	34	6.44	31	1.31	1	0.7	2
PTEN	4.04	34	6.86	33	1.31	1	NA	NA
SMARCA4	4.04	34	3.74	18	7.89	6	3.53	10
MSH2	3.92	33	4.36	21	2.63	2	3.53	10
SYK	3.92	33	4.78	23	2.63	2	2.82	8
RARA	3.8	32	4.57	22	2.63	2	2.82	8
UBR5	3.8	32	5.4	26	2.63	2	1.41	4
MAP2K1	3.69	31	6.23	30	1.31	1	NA	NA
CHD8	3.45	29	3.32	16	NA	NA	4.59	13
HVCN1	3.45	29	3.32	16	3.94	3	3.53	10
IKBKB	3.45	29	5.19	25	1.31	1	1.06	3
LYN	3.45	29	4.78	23	3.94	3	1.06	3
RUNX1	3.45	29	3.53	17	6.57	5	2.47	7
GRB2	3.33	28	4.36	21	2.63	2	1.76	5
HRAS	3.33	28	2.91	14	11.84	9	1.76	5
PRPS1	3.33	28	5.61	27	1.31	1	NA	NA
YY1	3.33	28	4.78	23	6.57	5	NA	NA
MTOR	3.21	27	5.4	26	NA	NA	0.35	1
DNMT3A	3.09	26	3.11	15	6.57	5	2.12	6
JUNB	3.09	26	3.32	16	10.52	8	0.7	2
TLR2	2.97	25	4.57	22	NA	NA	1.06	3
FBXW7	2.85	24	4.36	21	NA	NA	1.06	3
RAD9A	2.85	24	2.7	13	6.57	5	2.12	6
ANKRD17	2.73	23	4.36	21	1.31	1	0.35	1
ZBTB7A	2.73	23	2.07	10	9.21	7	2.12	6
ARID5B	2.61	22	4.36	21	NA	NA	0.35	1

CD22	2.61	22	3.32	16	2.63	2	1.41	4
NF1	2.61	22	3.11	15	2.63	2	1.76	5
IGLL5	2.38	20	1.03	5	17.1	13	0.7	2
KCMF1	2.38	20	3.32	16	2.63	2	0.7	2
PIK3R1	2.38	20	1.24	6	2.63	2	4.24	12
RRAGC	2.38	20	3.95	19	1.31	1	NA	NA
HNRNPD	2.26	19	3.74	18	NA	NA	0.35	1
JAK1	2.26	19	3.74	18	NA	NA	0.35	1
SF3B1	2.26	19	3.11	15	1.31	1	1.06	3
CXCR4	2.14	18	2.7	13	6.57	5	NA	NA
NFKB2	2.14	18	3.32	16	1.31	1	0.35	1
TCL1A	2.14	18	3.53	17	NA	NA	0.35	1
JAK3	2.02	17	1.24	6	10.52	8	1.06	3
CCL4	1.9	16	1.45	7	3.94	3	2.12	6
CHD1	1.9	16	2.7	13	NA	NA	1.06	3
FUT5	1.9	16	1.24	6	6.57	5	1.76	5
COQ7	1.78	15	1.87	9	1.31	1	1.76	5
GNAS	1.78	15	1.24	6	6.57	5	1.41	4
BTBD3	1.66	14	1.45	7	1.31	1	2.12	6
NANOG	1.66	14	1.24	6	3.94	3	1.76	5
PPP4R3A	1.66	14	2.49	12	1.31	1	0.35	1
CASP8	1.54	13	1.45	7	3.94	3	1.06	3
MAP4K4	1.54	13	2.07	10	2.63	2	0.35	1
STAT5B	1.54	13	0.83	4	2.63	2	2.47	7
LIN54	1.07	9	1.66	8	NA	NA	0.35	1
ZNF423	1.07	9	1.66	8	NA	NA	0.35	1
DICER1	0.95	8	1.45	7	1.31	1	NA	NA
FUBP1	0.95	8	1.45	7	1.31	1	NA	NA
GOLGA5	0.83	7	1.45	7	NA	NA	NA	NA

Supplementary Table 4. Clinical characteristics for patients in the MSKCC cohort.

Characteristic	N = 69[1]
Pre-CAR-T Age	67 (56, 73)
Sex	
Male	46 (67%)
Female	23 (33%)
Karnofsky Perfomance Status	
>=90	18 (26%)
<90	51 (74%)
LBCL subtype	
DLBCL NOS	55 (80%)
Other LBCL	5 (7.2%)
High-grade B-cell Ly.	9 (13%)
Double/Triple Hit	
Not Double/Triple Hit	58 (89%)
Double/Triple Hit	7 (11%)
Unknown	4
Transformed lymphoma	26 (38%)
Cell of Origin	
non-GCB	37 (54%)
GCB	32 (46%)
Pre-lymphodepletion LDH (ULN)	
normal	31 (45%)
elevated	38 (55%)
History of auto-HCT	19 (28%)
Pre-apheresis treatment lines (categorized)	
<=3 lines	38 (55%)
4-5 lines	18 (26%)
6+ lines	13 (19%)
Primary refractory disease (pre-apheresis)	26 (38%)
Bridging	57 (83%)
CAR-T product	
Axicabtagene ciloleuce	36 (52%)
Tisagenlecleucel	24 (35%)
Lisocabtagene maraleucel	9 (13%)

[1]Median (Q1, Q3); n (%); LDH- lactate dehydrogenase; ULN – upper limit of normal; auto-HCT – autologous heatopoeitic cell transplantation

Supplementary Methods

Data sets

NCI cohort: RNA-sequencing counts for 481 DLBCL biopsies were downloaded from dbGaP (phs001444)[1]. All patients had variants calls from whole exome sequencing and copy number arrays.

UCMC cohort: RNA-sequencing was performed on 96 DLBCL biopsies (84 treatment-naïve, 12-relapsed/refractory, 2 unknown). Paired whole exome sequencing was successful for 76 cases.

BCC cohort: RNA-sequencing counts for 285 treatment-naive DLBCL biopsies was provided by BCC[2,3]. Of these, 283 patients had available variant calls from targeted sequencing and copy number arrays.

Stanford cohort: RNA-sequencing for 88 DLBCL and HGBL biopsies were downloaded from dbGaP (phs003145.v1.p1)[4].

Genentech cohort : RNA-sequencing was performed on 74 pre-treatment DLBCL biopsies. All data requests can be directed to epenuel@gene.com.

MSKCC cohort: Exome-capture RNA-sequencing was performed on 69 FFPE sections from LBCL specimens collected within 1 year prior to CAR-T infusion **(Supplementary Table 4)**. All data requests can be directed to shouvalr@mskcc.org.

Molecular and genetic subtype classifications

Cell of origin: COO classifications were compiled from previously described gene expression-based classifiers. For the NCI cohort, all DLBCLs had COO calls from a DGE-based classifier[5]. For the BCC cohort, 283 DLBCLs had COO calls from Lymph3Cx[2]. For the UCMC cohort, all samples had COO calls from an RNAseq-based classifier from BostonGene[6].

***LME classifications*:** Lymphoma Microenvironment (LME) classifications for DLBCLs in the NCI, BCC, and UCMC cohorts were provided by BostonGene[6].

***LymphGen* classifications:** LymphGen classifications for the BCC and NCI cohorts were obtained from Wright et al.[1].

***Dark zone signature*:** DZsig (formerly known as double hit signature) classifications for the BCC and NCI cohorts were obtained from Ennishi et al. [3] and Wright et al. [1], respectively. DZsig classifications for the UCMC cohort were provided by BostonGene from an RNAseq-based classifier[6].

Generation and processing of sequencing data

Quality control: FastQC and FastQ Screen were used to assess read quality and other species contamination (www.bioinformatics.babraham.ac.uk). SNP (single nucleotide polyphorism)-calling using pileup in FACETS was used to assess sample mix-ups and contamination[7].

Mutation-calling and annotation: Whole exome sequencing data for the UCMC cohort was generated as previously described[8]. Mutation-calling for whole exome sequencing data for the UCMC cohort was performed similarly to the analysis in Kotlov et al [6]. Reads were trimmed using fastp to eliminate low-quality reads and then were aligned to the GRCh38 reference genome using BWA (v0.7.17)[9,10]. Duplicate reads were removed using Picard's MarkDuplicates (v2.6.0) ("Picard Toolkit", 2019. Broad Institute, GitHub Repository) and recalibrated by BaseRecalibrator and ApplyBQSR from GATK4[11]. For samples with a paired normal reference, short variants were called using Strelka[12]. For tumor-only samples, Pisces (v5.2) was used[13]. Variants were annotated using Variant Effect Predictor (VEP)[14]. For all data sets, variants were restricted to these predicted to be deleterious.

Copy number analysis: Copy number variation (CNV) was assessed using Sequenza with modifications from FACETS[7,15]. CNV analysis was performed in the space of genes listed in **Supplementary Table 2.** Sequenza input reference was modified to match FACETS, calculated using facets-pileup. For tumor-only samples, calling versus average normal or tumor sample was performed using a modified version of Sequenza. Average normal/tumor pileup files were prepared to average normalized coverage and variant allele fraction (VAF) at each position. Some samples were excluded due to low coverage and/or tumor content. For all data sets, heterozygous deletions and low-level copy gains were excluded.

RNA-seq processing and normalization: Paired-end and single-end RNA-seq data for the UCMC cohort was generated as previously described[8]. RNA-seq reads were aligned using kallisto v0.42.4 to GENCODE v23 transcripts with default parameters[16]. The protein-coding transcripts, immunoglobulin heavy, kappa and lambda light chains, and TCR-related transcripts were retained; noncoding RNA, histone, and mitochondria-related transcripts were removed. Counts were processed using limma (v3.52.4) and edgeR (v3.38.4). Genes with low counts were removed using a threshold of a 0.5 log2CPM average across all samples, as previously described[17]. Then, TMM (trimmed mean of M-values) normalization was performed, and counts were quantified as log2CPM. Batch correction was performed using the removeBatchEffect function in limma.

For DLBCLs in the mosunetuzumab cohort, robust library sizes were estimated using DESeq2, and raw RNASeq counts were normalized via limma-voom.

For the MSKCC cohort, FFPE sections from tissue specimens collected within 1 year prior to CAR-T infusion were deparaffinized in mineral oil. Nucleic acids were isolated using the AllPrep DNA/RNA Mini Kit (QIAGEN, Cat #:80204) according to the manufacturer's instructions. FFPE

RNA was used for RNA library construction using the KAPA RNA Hyper library prep kit (Roche) per the manufacturer's instructions with minor modifications. Customized adapters with unique molecular indexes (UMI; Integrated DNA Technologies) and sample-specific dual-index primers (Integrated DNA Technologies) were added to each library. Equal amounts of each RNA library were pooled for hybridization capture with IDT Whole-Exome Panel V2 (Integrated DNA Technologies) using a customized capture protocol modified from the NimbleGen SeqCap Target Enrichment system (Roche). The captured DNA libraries were then sequenced on an Illumina HiSeq4000 with paired end reads (2Å ~ 100 bp), at 50 million reads/sample.

Read mapping was done using Kallisto[16]. Kallisto quantification files were processed to generate a gene-level expression matrix for downstream analysis. Transcript-to-gene mapping was performed using the Ensembl GRCh37 BioMart database, retrieving transcript IDs and their corresponding gene symbols[14]. Transcript-level quantifications from Kallisto were then imported using the tximport package, with transcript data summarized to the gene level based on the BioMart mapping. Length-scaled TPM values were used to estimate counts, and transcript versioning was ignored to ensure consistency.

Differential gene expression (DGE) and gene set enrichment analysis (GSEA):

DGE was performed using voom, and differentially expressed genes were generally defined as those with $|\log2FC| \geq 1$ and adjusted p value < 0.05[18]. GSEA was performed using the Desktop client (v4.2.3) with default settings[19].

Mutational pathway analysis

Genes in the BCR-dependent NFKB pathway[20,21] and cell cycle pathway-related genes[21] were curated from previously published studies. The proportion of patients with an alteration in at least one gene in the pathway was calculated and compared across clusters. Alterations for a given gene were filtered to reflect their putative role as an oncogene or as a tumor suppressor gene.

CIBERSORTx

Immune cell deconvolution was performed using CIBERSORTx using the LM22 signature matrix[22,23]. The software was run on bulk-mode and absolute mode. For the input mixture file, RNA-seq counts were first batch corrected using ComBat-Seq followed by quantification to transcripts per million (TPM)[24].

Cell types were condensed as such:

T.cells = "T cells CD8" + "T cells follicular helper (T_{fh})" + "T cells regulatory (Tregs)" + "T cells CD4 naïve" + "T cells CD4 memory resting" + "T cells CD4 memory activated"+ "T cells gamma delta"

NK.cells = "NK cells activated" + "NK cells resting"

Memory.CD4.T.cells = "T cells CD4 memory resting" + "T cells CD4 memory activated"

Conv.CD4.T.cells = "Memory.CD4.T.cells" + "T cells CD4 naïve" + "T cells follicular helper"

CD4.T.cells = "Memory.CD4.T.cells" + "T cells CD4 naïve" + "T cells follicular helper" + "T cells regulatory (T_{regs})"

Dendritic.cells = "Dendritic cells activated" + "Dendritic cells resting"

B.cells = "B cells naïve" + "B cells memory" + "Plasma cells"

Macrophages = "Macrophages M0" + "Macrophages M1" + "Macrophages M2"

EcoTyper (https://github.com/digitalcytometry/ecotype) was used to recover previously defined Lymphoma Ecotypes; input data were quantified as TPM[25].

Generation of MYCUp4 expression groups

GSVA scores for the MYCUp-4 gene set (from SigDB[26]) were generated for all DLBCLs in UCMC, NCI, and BCC datasets. DLBCLs were then split into ABC and GCB groups based on their immune-related cluster membership, and a 25-75 percentile split within each COO group was used to assign DLBCLs to "MYC-High" and "MYC-Low" groups. All other DLBCLs were assigned to the "MYC-Int" group.

Multispectral immunofluorescence

Multi-spectral immunofluorescence (mIF) microscopy was performed on 65 DLBCLs (UCMC) for which paired RNA-seq and GSVA data were available. mIF analysis was performed after staining with fluorescence-labeled antibodies against a T cell panel and myeloid cell panel *(see antibodies for mIF section*). Each slide was scanned using the Vectra Polaris (Akoya Biosciences) imaging platform and the Phenochart software (PerkinElmer). Through Phenochart, at least 5 representative regions of interest per tissue section were acquired as multispectral images at 40x magnification. Watershed segmentation was used to identify nuclei using DAPI staining and cell borders of individual cells in each ROI. The supervised machine-learning algorithm in the inForm software (v. 2.3) was used to classify each cell into specific phenotypes.

1. Slides were divided by panel and by specific features determined during the initial watershed segmentation, including cell border detection, average cell size, autofluorescence, and DAPI strength.

2. Samples were divided into 4 separate groups for each panel. 2 ROIs were chosen per sample to train the machine-learning algorithm in inForm to identify the following phenotypes with the associated markers:
    1. **T cells** : $CD8^+$ T cell, $CD4^+$ T cell, $PAX5^+$ DLBCL cell
    2. **Myeloid cells** : $CD68^+$ Macrophage, $CD11c^+$ dendritic cell
3. Once the initial training groups were processed, all ROIs in each group of samples were classified using the matching training cohort.
4. Results of per-slide frequencies of each phenotype were tabulated in R using exported values from inForm using the `phenoptr` package and the representative mIF images were also exported through inForm. Given heterogeneity of tumor and microenvironment composition in each ROI, comparisons were made between total number of each TME cell population/phenotype normalized against the number of DLBCL cells present across all ROIs per slide.

Antibodies for mIF

PAX5	nucleus	620	BioCare Medical,CM 207	BC/24, mouse mAb	AR9	1:50 in Da Vinci Green
CD68	membrane+cytoplasmic	570	BioCare Medical, CM033A	KP1, mouse mAb	AR9	1:50 in Da Vinci Green
CD11c	membrane	540	BioCare Medical, ACI3122A	5D11, mouse mAB	AR9	1:100 in Renoir Red

CD4	membrane	520	BioCare Medical, ACI3148A	4B12, mouse mAb	AR9	1:50 in Van Gogh Yellow
PAX5	nucleus	620	BioCare Medical,CM 207	BC/24, mouse mAb	AR9	1:50 in Da Vinci Green
CD8	membrane	690	R&D, NBP232836B	C8/144B, mouse mAb	AR9	1:50

***In vitro* IFNγ stimulation of splenocytes**

Spleens from *CD19*$^{Cre/wt}$ and *CD19*$^{Cre/wt}$; *Socs1*$^{fl/fl}$ mice were obtained from Ari Melnick (Weill Cornell Medicine). Spleens were passed through a 70 µm cell strainer (Corning, 352350) and ground using the plunger of a syringe with 10 mL of PBS to yield single cell suspensions. Splenocytes were then washed twice in 10mL of PBS, followed by lysis of red blood cells in a hypotonic solution and three washes in 10 mL of PBS. 5 x 10^5 splenocytes from single cell suspensions were incubated with increasing concentrations of recombinant mouse IFNγ (0, 0.1, 1, 10, 100 ng/mL) for 48 hours (Peprotech, 315-05). Cells were then harvested and incubated with a panel of antibodies containing anti-mouse CD19 (Biolegend,115504), anti-mouse CD3d (Biolegend, 100244), anti-mouse H-2 (Biolegend, 125506), anti-mouse I-A/I-E (Biolegend, 107619), and anti-mouse PD-L1 (Biolegend, 124311). Splenocytes were analyzed by flow cytometry for expression of H-2, I-A/I-E, and PD-L1 on $CD19^+$ and $CD3^+$ cell populations. Mean fluorescence intensity (MFI) fold change for H-2, H-2, I-A/I-E, and PD-L1 was computed by comparing treatment with IFNγ compared to media-only control. Data shown are the average of at least 3 independent biological replicates. Statistical testing was conducted using a 2-way ANOVA with Bonferroni correction for multiple comparisons.

Supplementary References

1. Wright GW, Huang DW, Phelan JD, et al. A Probabilistic Classification Tool for Genetic Subtypes of Diffuse Large B Cell Lymphoma with Therapeutic Implications. *Cancer Cell*. 2020;37(4):551-568.e14.
2. Duns G, Viganò E, Ennishi D, et al. Characterization of DLBCL with a PMBL gene expression signature. *Blood*. 2021;138(2):136–148.
3. Ennishi D, Jiang A, Boyle M, et al. Double-Hit Gene Expression Signature Defines a Distinct Subgroup of Germinal Center B-Cell-Like Diffuse Large B-Cell Lymphoma. *JCO*. 2019;37(3):190–201.
4. Sworder BJ, Kurtz DM, Alig SK, et al. Determinants of resistance to engineered T cell therapies targeting CD19 in large B cell lymphomas. *Cancer Cell*. 2023;41(1):210-225.e5.
5. Wright G, Tan B, Rosenwald A, et al. A gene expression-based method to diagnose clinically distinct subgroups of diffuse large B cell lymphoma. *Proceedings of the National Academy of Sciences of the United States of America*. 2003;100(17):9991–9996.
6. Kotlov N, Bagaev A, Revuelta MV, et al. Clinical and Biological Subtypes of B-cell Lymphoma Revealed by Microenvironmental Signatures. *Cancer Discovery*. 2021;11(6):1468–1489.
7. Shen R, Seshan VE. FACETS: allele-specific copy number and clonal heterogeneity analysis tool for high-throughput DNA sequencing. *Nucleic Acids Research*. 2016;44(16):e131.
8. Godfrey J, Tumuluru S, Bao R, et al. PD-L1 gene alterations identify a subset of diffuse large B-cell lymphoma harboring a T-cell–inflamed phenotype. *Blood*. 2019;133(21):2279–2290.
9. Chen S, Zhou Y, Chen Y, Gu J. fastp: an ultra-fast all-in-one FASTQ preprocessor. *Bioinformatics*. 2018;34(17):i884–i890.
10. Li H, Durbin R. Fast and accurate short read alignment with Burrows-Wheeler transform. *Bioinformatics*. 2009;25(14):1754–1760.
11. Van der Auwera GA, Carneiro MO, Hartl C, et al. From FastQ data to high confidence variant calls: the Genome Analysis Toolkit best practices pipeline. *Curr Protoc Bioinformatics*. 2013;11(1110):11.10.1-11.10.33.
12. Saunders CT, Wong WSW, Swamy S, et al. Strelka: accurate somatic small-variant calling from sequenced tumor–normal sample pairs. *Bioinformatics*. 2012;28(14):1811–1817.
13. Dunn T, Berry G, Emig-Agius D, et al. Pisces: an accurate and versatile variant caller for somatic and germline next-generation sequencing data. *Bioinformatics*. 2019;35(9):1579–1581.
14. McLaren W, Gil L, Hunt SE, et al. The Ensembl Variant Effect Predictor. *Genome Biology*. 2016;17(1):122.
15. Favero F, Joshi T, Marquard AM, et al. Sequenza: allele-specific copy number and mutation profiles from tumor sequencing data. *Annals of Oncology*. 2015;26(1):64–70.
16. Bray NL, Pimentel H, Melsted P, Pachter L. Near-optimal probabilistic RNA-seq quantification. *Nat Biotechnol*. 2016;34(5):525–527.
17. Hänzelmann S, Castelo R, Guinney J. GSVA: gene set variation analysis for microarray and RNA-Seq data. *BMC Bioinformatics*. 2013;14(1):7.
18. Law CW, Chen Y, Shi W, Smyth GK. voom: precision weights unlock linear model analysis tools for RNA-seq read counts. *Genome Biology*. 2014;15(2):R29.
19. Subramanian A, Tamayo P, Mootha VK, et al. Gene set enrichment analysis: a knowledge-based approach for interpreting genome-wide expression profiles. *Proceedings of the National Academy of Sciences of the United States of America*. 2005;102(43):15545–50.
20. Phelan JD, Young RM, Webster DE, et al. A multiprotein supercomplex controlling oncogenic signalling in lymphoma. *Nature*. 2018;560(7718):387–391.

21. Miao Y, Medeiros LJ, Li Y, Li J, Young KH. Genetic alterations and their clinical implications in DLBCL. *Nat Rev Clin Oncol*. 2019;16(10):634–652.
22. Newman AM, Steen CB, Liu CL, et al. Determining cell type abundance and expression from bulk tissues with digital cytometry. *Nature Biotechnology*. 2019;37(7):773–782.
23. Newman AM, Liu CL, Green MR, et al. Robust enumeration of cell subsets from tissue expression profiles. *Nat Methods*. 2015;12(5):453–457.
24. Zhang Y, Parmigiani G, Johnson WE. ComBat-seq: batch effect adjustment for RNA-seq count data. *NAR Genom Bioinform*. 2020;2(3):lqaa078.
25. Steen CB, Luca BA, Esfahani MS, et al. The landscape of tumor cell states and ecosystems in diffuse large B cell lymphoma. *Cancer Cell*. 2021;
26. Shaffer AL, Wright G, Yang L, et al. A library of gene expression signatures to illuminate normal and pathological lymphoid biology. *Immunological Reviews*. 2006;210(1):67–85.